Central-Field Intermolecular Potentials from the Differential Elastic Scattering of $H_2(D_2)$ by other Molecules *

BY ARON KUPPERMANN, ROBERT J. GORDON† AND MICHAEL J. COGGIOLA‡
Arthur Amos Noyes Laboratory of Chemical Physics,§

California Institute of Technology, Pasadena, California 91109

Received 26th February, 1973

Differential elastic scattering cross sections for the systems H_2+O_2, SF_6, NH_3, CO, and CH_4 and for D_2+O_2, SF_6, and NH_3 have been obtained from crossed beam studies. In all cases, rapid quantum oscillations have been resolved which permit the determination of intermolecular potential parameters if a central-field assumption is adopted. These potentials were found to be independent of both the isotopic form of the hydrogen molecule, and the relative collision energy. As a result of this, and the ability of these spherical potentials quantitatively to describe the measured scattering, it is concluded that anisotropy effects do not seem to be important in these $H_2(D_2)$ systems.

The determination of interatomic and intermolecular potentials from molecular beam experiments has received considerable attention over the last few years. Early experiments at high energy with various atomic,[1] ionic,[2] and molecular [3] systems yielded essentially structureless total cross sections. In order to determine the scale of the potential from such data, it is essential to have absolute cross sections,[4] which require accurate calibration of beam intensities. It has long been recognized that the calibration problem can be avoided if the cross section has structural features that provide an internal "calibration." Recently, rapid quantum oscillations have been resolved in differential elastic cross sections,[5-9] which provide the necessary calibration. The frequency of such undulations has been related,[10] for central-field potentials, to the range of the potential according to the approximate expression

$$\Delta\theta \approx (\pi\hbar/\mu v\sigma) \approx (\lambda/2\sigma) \tag{1}$$

where $\Delta\theta$ is the spacing of the oscillations, μ is the reduced mass, v is the relative collision velocity, σ is a range parameter for the potential (e.g., the zero of the potential), and λ is the de Broglie wavelength. As a result, well resolved rapid oscillations permit the estimation of σ independently of the shape and depth of the potential well. A more quantitative fit to experiment of the differential cross sections calculated from an assumed potential permits one to determine more quantitatively this potential for systems subject to central forces. In particular, information about the depth of the attractive well and the steepness of the repulsive part of the potential can be obtained.

Partly because of the simplicity of interpreting the experiments for central fields, most of the measurements of quantum oscillations have been for atom-atom scattering.

* Work supported in part by the U.S. Atomic Energy Commission, Report Code No. CALT-767P4-112.

† present address: Naval Research Laboratory, Washington, D.C.

‡ Work performed in partial fulfilment of the requirements for the Ph.D. Degree in Chemistry at the California Institute of Technology.

§ Contribution No. 4650.

The first molecular system found to have oscillations given by (1) was D_2+N_2, reported by Winicur *et al.*[6] In the present study, which is a continuation of their work, we have measured the differential elastic cross sections of D_2 and H_2 scattered by O_2, CO, NH_3, CH_4, and SF_6, in order to obtain information about the corresponding intermolecular potentials. The data are discussed from the perspective of a central field approximation. Variation of the relative collision energy and the use of both H_2 and D_2 with the same scattering partner provide a useful test for the validity of this approximation.

Some of the systems reported here have also been studied in total cross section experiments by Butz *et al.*[11] and by Aquilante *et al.*[12] Information obtained from total and differential cross section measurements on the same systems are mutually complementary.

EXPERIMENTAL

The crossed molecular beam apparatus is shown schematically in fig. 1 and 2. The main features of the machine are a movable, differentially pumped quadrupole mass spectrometer detector, a differentially pumped supersonic primary beam and a subsonic secondary beam perpendicular to the primary beam, all contained in a bakeable stainless steel 1200 l. main vacuum chamber. The beams intersect the axis of the main chamber at the centre of rotation of the detector. The detector chamber is mounted on a semicircular shaped quadrant arm which pivots about the axis of the main chamber, while the detector is free to move along the rim of the quadrant out of the plane of the beams. Thus the detector can scan both colatitudinal and longitudinal angles, although only in-plane measurements were made in the present experiments. Pumping in the main chamber is by means of four 6 in. oil diffusion pumps, each having a nominal trapped speed of 1250 l./s, and a liquid nitrogen cooled titanium sublimation pump, with a calculated speed of 20 000 l./s for air. The primary beam source chamber and buffer are pumped by a 6 in. oil diffusion pump (1250 l./s) and a 6 in. mercury diffusion pump (150 l./s), respectively.

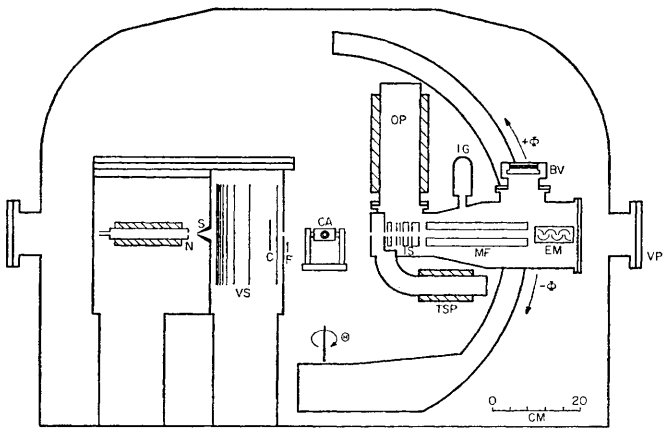

FIG. 1.—Vertical cross section of molecular beam apparatus. N—primary nozzle source, S—skimmer cone, VS—velocity selector, C—primary beam chopper, F—beam flag, CA—secondary beam glass capillary array, IS—electron bombardment ionizer, MF—quadrupole mass filter, EM—electron multiplier, TSP—titanium sublimator pump, OP—Orbion pump, IG—ionization gauge, BV—bellows operated bakeout valve, VP—Pyrex view port.

All apertures in the apparatus are circular, with the entrance aperture of the detector housing (0.16 cm diam.) located 8.05 cm away from the intersection of the beams. The exit aperture of the primary beam chamber (0.21 cm diam.) is located 7.9 cm away from the

scattering centre, and the secondary effusive source (0.16 cm diam.) is 0.5 cm from the centre. The primary beam is formed with the aid of a nozzle-skimmer arrangement giving a measured Mach number of ~ 15 and an angular FWHM (full width at half maximum) of 1.4°. A jacket surrounding the nozzle tube permits one to cool the entire nozzle assembly to liquid nitrogen temperature.

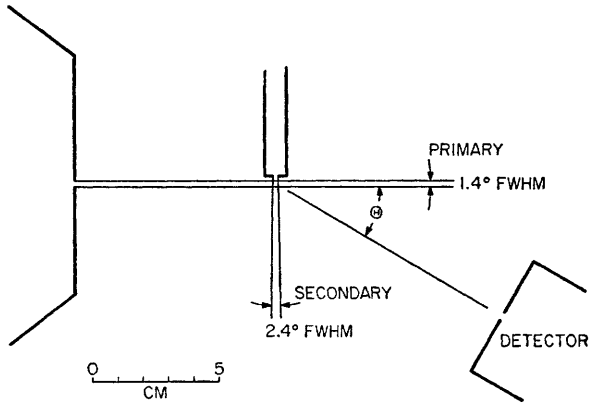

FIG. 2.—Crossed beam geometry. Θ is the measured laboratory scattering angle.

The secondary beam source consists of a glass capillary array attached to the end of a brass tube, which can be tilted out of the plane of the beams by pumping the air out of a stainless steel bellows attached to this source. When the secondary source is tilted, the two beams do not cross, and the background signal intensity can be measured. This procedure is superior to flagging the secondary beam since the latter method tends to modulate the background as well as the signal. The angular width of the secondary beam is 2.4° FWHM. The FWHM cross section of the beam intersection region in the collision plane has the approximate shape of a rectangle 0.17 cm along the direction of the primary beam and 0.22 cm along the direction of the secondary beam. The angular resolution of the detector is approximately 2°.

The heart of the apparatus is an Extranuclear 324-9 quadrupole mass spectrometer [13] mounted in a bakeable double differentially pumped chamber. The operating pressure in the ionization region, measured with an uncalibrated Bendix miniature ionization tube, is typically 2×10^{-9} Torr with the beams on, whereas in the main chamber, it is about 1×10^{-6} Torr under these conditions. To obtain such a large pressure differential, we found it necessary to bake the spectrometer housing and Orbion pump for about 8 h at approximately 200°C whenever the machine was pumped down from atmospheric pressure. The mass spectrometer chamber is equipped with a bellows activated valve 6 cm in diameter which is kept open to the main chamber during the bake-out period in order to accelerate the removal of background gas.

Particles entering the mass spectrometer chamber pass successively through a high-efficiency electron impact ionizer, a series of electrostatic focusing lenses, and a 23 cm long Paul [14] quadrupole mass filter. Ions are detected by a 14 stage CuBe electron multiplier whose output is amplified by an Extranuclear tuned amplifier followed by a Princeton Applied Research HR-8 phase sensitive detector. The amplified signal is finally converted to digital form by a Raytheon model ADC-24 analog-to-digital converter.

The apparatus is interfaced to an SCC-4700 computer, which serves several functions. First, it tilts the secondary beam in (" on " mode) and out (" off " mode) of the scattering plane. Second, the computer periodically samples and averages the amplified signal and subtracts the background from the total intensity. Third, it calculates the standard deviations for both " on " and " off " modes.

The signal to noise ratio varied from better than 100 at the small scattering angles to a

minimum of 10 at the largest one. To correct for long term drift in the signal caused by such factors as fluctuations of beam intensities and gradual build-up of background in the mass spectrometer, a fixed scattering angle (generally between 3.0° and 5.0°) was chosen as a reference angle. After the measurement of the signal at each scattering angle, the intensity at the reference angle was remeasured to provide a normalization factor. In this way, individual relative intensity points were reproducible to within 5 % when remeasured on different days.

RESULTS

The differential cross sections for the systems H_2+O_2, SF_6, CO, NH_3, CH_4 and D_2+O_2, SF_6, NH_3, were all measured using room temperature H_2 and D_2 beams, with a relative collision energy of approximately 0.06 eV. Measurements of the H_2+SF_6 and H_2+NH_3 systems were also made using an H_2 beam cooled to liquid nitrogen temperature, with a relative energy of approximately 0.02 eV. In addition, the SF_6 system was studied using a low temperature beam of para-hydrogen. These experiments scan a wide range in the size, anisotropy and initial relative collision energy of the scattering species, and of the corresponding de Broglie wavelengths. The measured differential elastic cross sections are shown in fig. 3 to 7 inclusive, together with the on-line computer determined error bars. The various curves drawn through the measured points were fitted to the data as described below.

DETERMINATION OF THE INTERMOLECULAR POTENTIAL

In the interpretation of our data we have assumed that the differential elastic cross sections measured are due to the spherically symmetric part of the intermolecular potentials. The reason for this assumption and the tests of its validity are described in the Discussion. In our analysis, a model potential function is assumed and the potential parameters are varied until a least-squares fit of theory to experiment is obtained.

In the present analysis we have used a Lennard-Jones (n, 6) potential, where the repulsive exponent n was either fixed at 12 or 20, or was allowed to vary as a fitted parameter. In addition, a Morse-cubic spline-van der Waals (MSV) potential [15] was used in some systems. The MSV potential is defined by

$$V(r) = \begin{cases} \varepsilon\{\exp[-2\beta(r-r_m)]-2\exp[-\beta(r-r_m)]\} & r<r_1 \\ \text{cubic spline} & r_1 \leqslant r \leqslant r_2 \\ -C_6 r^{-6} & r_2 < r \end{cases}$$

The cubic spline function is a set of five cubic polynomials whose coefficients are chosen to smoothly join the inner and outer branches of the potential. The end points were taken such that $V(r_1) = -0.75\,\varepsilon$, and $r_2 = r_1 + 0.2\,r_m$. The fitting parameters were ε, r_m, β and C_6. The corresponding differential cross sections were accurately calculated using a partial wave expansion employing both JWKB and high energy eikonal phase shifts, tested against accurate integration of the radial Schrödinger equation to assure the validity of this method. In order to compare the computed cross sections with the data, it is necessary to correct for velocity spread and angular resolution of the apparatus. In trial calculations, we found that the former effect tends to dampen the undulations at CM scattering angles $> 15°$ while the latter dampens the small angle scattering to roughly an equal extent. This situation differs from that of Siska *et al.*[15] who found that under their experimental conditions with both beams supersonic, the effect of angular resolution was dominant at all scattering angles and that they could lump both corrections into a single effective angular resolution function. Consequently, the calculated cross sections were transformed to the

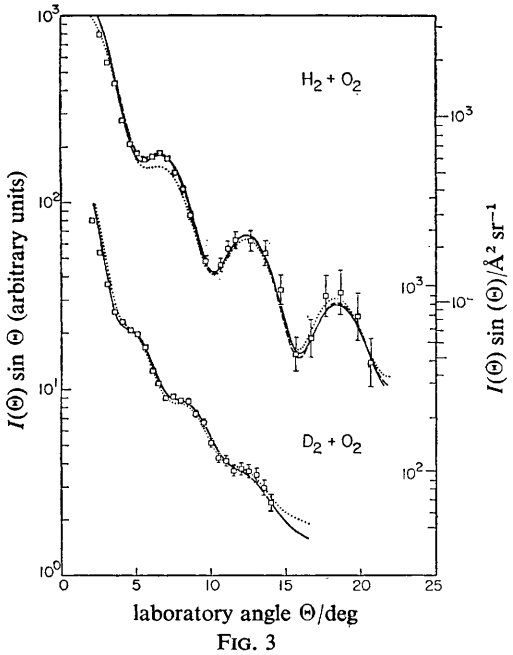

FIG. 3

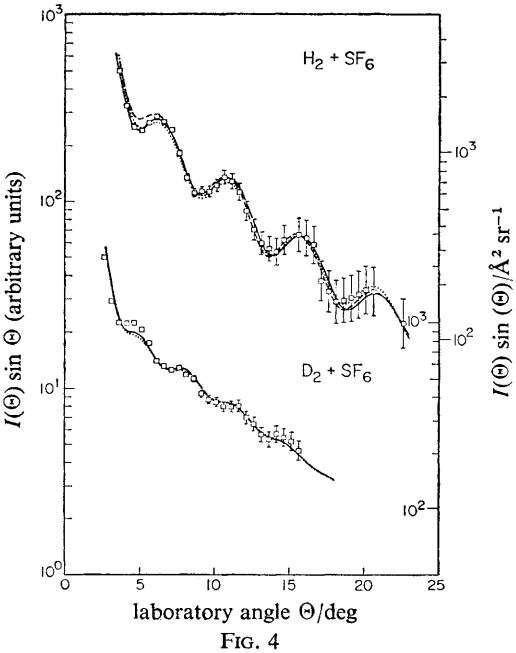

FIG. 4

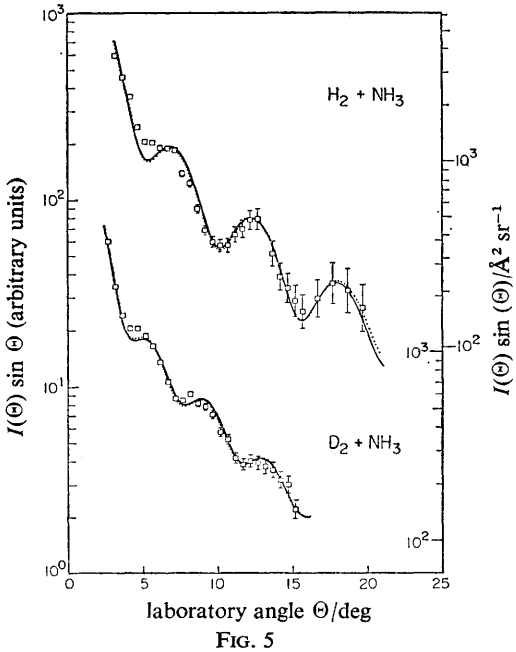

FIG. 5

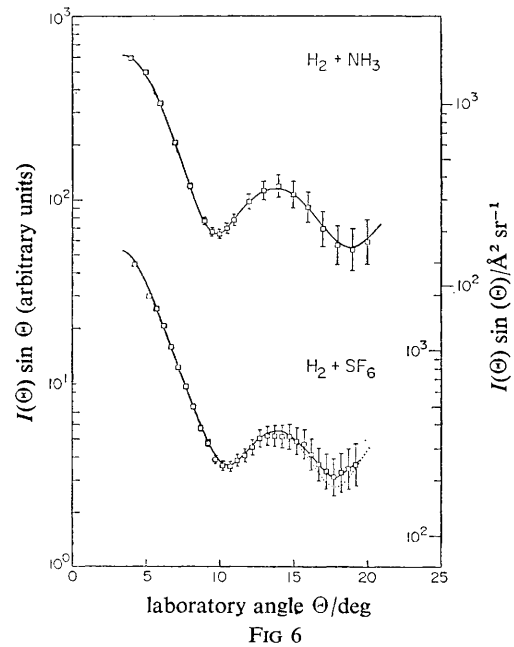

FIG 6

FIG. 3.—Plot of the product of the scattered intensity I times the sine of the angle Θ against Θ in the laboratory system of reference for H_2+O_2 and D_2+O_2 collisions. The lower curve has been shifted downwards by one decade. Points are experimental, and curves are theoretical fits. The solid curves are the MSV fits, and the corresponding potentials were used to establish the outer and inner ordinate scales for the H_2+O_2 and D_2+O_2 results, respectively. The upper dashed curve is the LJ (12, 6) fit, and the dotted curves are the LJ (n, 6) fits.

FIG. 4.—Differential scattering results for (room temperature) H_2+SF_6 and D_2+SF_6 collisions. Explanation of the curves is the same as fig. 3.

FIG. 5.—Differential scattering results for (room temperature) H_2+NH_3 and D_2+NH_3 collisions. Explanation of the curves as for fig. 3. The LJ (12, 6) fits were indistinguishable from the LJ (n, 6) ones and were not plotted.

FIG. 6.—Low temperature results for H_2+NH_3 and H_2+SF_6 collisions. Explanation of curves is given in fig. 3. The LJ (n, 6) curve for H_2+NH_3 was indistinguishable from the MSV curve and was not plotted. Results using para-hydrogen + SF_6 were identical to those shown for normal-hydrogen.

laboratory system and averaged over both the relative collision energy distribution and the detector angular resolution.

The potential parameters were fitted to the data by minimizing the weighted sum of squares of the differences between the cross sections calculated as just described and the experimental results, treating the vertical scale coefficient as a fitting parameter. For the Lennard-Jones potentials with n fixed, the fitted parameters ε and σ were found using a simple Newton's method. In the case of the MSV (ε, r_m, β, C_6) and the three parameter Lennard-Jones (ε, σ, n) potentials, a general method due to Marquardt [16] was used. In the following sections, the quoted values for the uncertainties of the potential parameters are those corresponding to a 95 % confidence level.

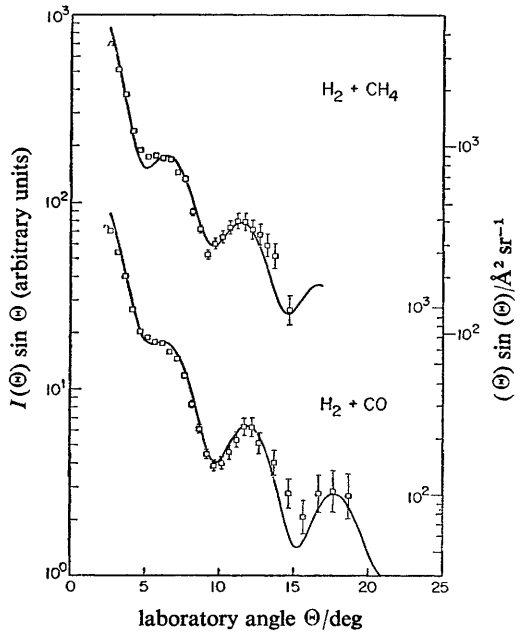

FIG. 7.—Differential scattering results for the $H_2 + CH_4$ and $H_2 + CO$ collisions. Only LJ (12, 6) fits were attempted, and they are shown by the solid curves.

All the systems were initially fitted with an LJ (12, 6) potential. The optimum values of ε and σ and their 95 % confidence levels are listed in table 1 together with λ, the de Broglie wavelength for each system, and Q the total cross section as calculated from the partial wave expansion. In addition, the results of the LJ (20, 6) and (n, 6) fits are also given in this table. The O_2, SF_6 and NH_3 data were measured with the most accuracy, and hence were chosen for the four parameter MSV fits. The $H_2 + CH_4$ and $H_2 + CO$ data were of poorer reproducibility quality and for this reason not submitted to such fits. The corresponding parameters are listed in table 2 together with the values for λ and Q. Various calculated differential cross sections are shown in fig. 3 to 7 inclusive. In all cases, the σ thus determined was within 10 % of the value predicted by eqn (1). It is worth emphasizing that while the statistical uncertainties in the fitted potential parameters listed in tables 1 and 2 are often quite small, it does not follow that the " true " values of these quantities (e.g., the actual well depth) must lie within the predicted ranges.

In fig. 8, 9 and 10 are shown fitted LJ and MSV potentials for the O_2, SF_6 and NH_3 data. In each case, the MSV and LJ potential with fitted repulsive parameter are given for the room temperature H_2 system, while only the MSV fit is given for the

TABLE 1.—LENNARD-JONES (n, 6) POTENTIAL PARAMETERS AND TOTAL CROSS SECTIONS

system	n	σ/Å	ε/meV	λ/Å	Q/Å^2
H_2+O_2	12	3.38±0.03	7.7±0.9	0.84	208±15
	13.2	3.40±0.04	7.2±0.9	0.84	182±12
	20	3.46±0.04	7.6±1.2	0.84	169±15
D_2+O_2	12	3.5±0.2	7.3±0.6	0.61	270±21
	13.6	3.5±0.3	7.0±0.7	0.61	251±20
	20	3.6±0.2	6.7±0.9	0.61	222±30
H_2+SF_6	12	4.05±0.06	10.4±0.5	0.81	380±41
	16.2	4.12±0.04	10.4±0.3	0.81	361±30
	20	4.15±0.04	10.4±0.8	0.81	335±31
	12	4.15±0.08	9.6±0.3	1.52	326±31
	16.3	4.18±0.05	10.0±0.2	1.52	325±28
	20	4.14±0.04	10.5±0.2	1.52	313±19
D_2+SF_6	12	4.2±0.4	10.3±0.6	0.58	380±32
	19.1	4.2±0.2	10.3±0.3	0.58	331±30
	20	4.2±0.2	10.3±0.4	0.58	334±31
H_2+NH_3	9.1	3.34±0.07	9.6±1.2	0.87	225±15
	12	3.45±0.06	9.8±1.4	0.87	260±18
	9.1	3.34±0.09	10.3±0.7	1.56	256±17
	12	3.34±0.08	10.3±0.8	1.56	255±17
D_2+NH_3	9.2	3.39±0.08	9.1±0.8	0.65	250±21
	12	3.26±0.07	9.1±0.7	0.65	245±21
H_2+CO	12	3.5±0.1	6.9±1.5	0.84	210±18
H_2+CH_4	12	3.7±0.2	9.9±1.4	0.87	317±26

corresponding D_2 systems. Those potentials not shown, were in general, indistinguishable from those which were plotted. In the case of the SF_6 and NH_3 systems, all three potentials are seen to be in very close agreement, while for the O_2 systems, the agreement is somewhat poorer. In all cases, however, the potentials overlap throughout the range plotted when the uncertainties in the potential parameters are taken into

TABLE 2.—MORSE–SPLINE–VAN DER WAALS (MSV) POTENTIAL PARAMETERS AND TOTAL CROSS SECTIONS

system	σ/Å	r_m/Å	ε/meV	β	C_6/eV Å^6	λ/Å	Q/Å^2
H_2+O_2	3.34±0.05	3.86±0.05	7.2±0.6	5.2±0.4	64.8±0.7	0.84	213±19
D_2+O_2	3.5±0.2	4.03±0.2	6.9±0.9	4.8±0.4	63.1±0.6	0.61	291±26
H_2+SF_6	4.14±0.02	4.63±0.02	10.0±0.2	6.5±0.5	57.2±0.3	0.81	396±33
	4.16±0.03	4.64±0.03	10.2±0.2	6.3±0.6	55.9±0.5	1.52	325±31
D_2+SF_6	4.2±0.2	4.62±0.2	10.4±0.8	6.6±0.6	54.6±0.5	0.58	389±38
H_2+NH_3	3.42±0.05	3.80±0.05	9.7±0.5	4.9±0.4	58.2±0.6	0.87	288±21
	3.23±0.05	3.88±0.05	10.2±0.5	4.8±0.4	59.2±0.7	1.56	242±20
D_2+NH_3	3.23±0.05	3.77±0.05	9.0±0.8	4.9±0.4	59.8±0.7	0.65	258±18

account. Hence, to within the experimental errors, the potentials for the H_2 and D_2 isotopes are the same for a given scattering partner, and the resulting potential is independent of the mathematical form chosen, and of the de Broglie wavelength. It

should be noted that agreement of the long range regions of the potentials is expected since both the LJ and MSV forms are chosen to have an r^{-6} dependence and, in addition, the measured scattering is not very sensitive to this region. The range of intermolecular distances sampled in these experiments, and depicted in fig. 8 to 10 inclusive, was approximately estimated by calculating the classical deflection function from the MSV potentials and considering the range of angles in the CM system covered for each system.

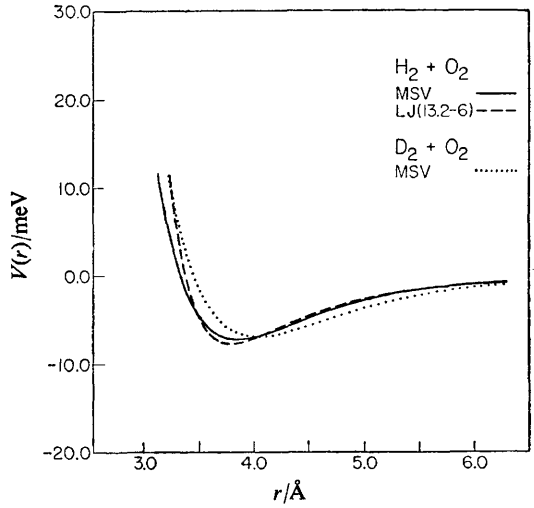

FIG. 8.—Comparison of the intermolecular potentials over the range of distances sampled for H_2+O_2 ($\lambda = 0.84$ Å) and D_2+O_2 ($\lambda = 0.61$ Å), determined from the data in fig. 3. The solid curve is the H_2+O_2 MSV potential, while the dashed curve is the H_2+O_2 LJ (n, 6) potential. The dotted curve represents the D_2+O_2 MSV potential.

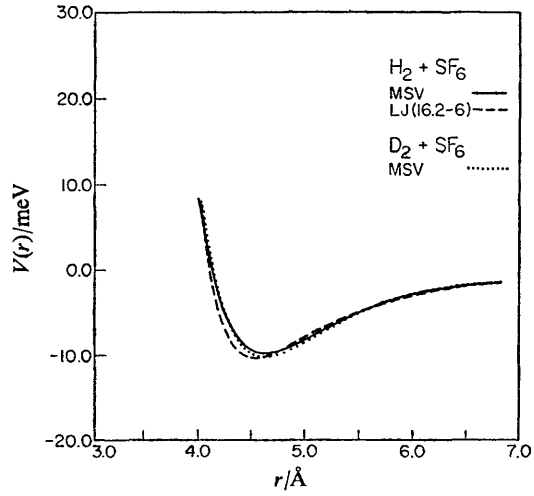

FIG. 9.—Comparison of the intermolecular potentials for H_2+SF_6 ($\lambda = 0.81$ Å) and D_2+SF_6 ($\lambda = 0.58$ Å). Explanation of the curves is given in fig. 8. The corresponding curves for H_2+SF_6 at $\lambda = 1.52$ Å are indistinguishable from those at $\lambda = 0.87$ Å, within plotting accuracy.

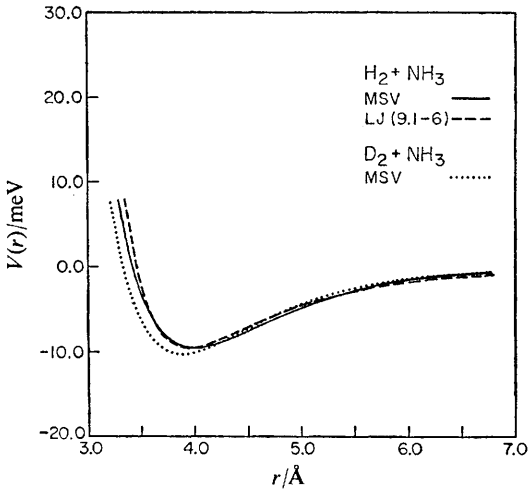

FIG. 10.—Comparison of the intermolecular potentials for H_2+NH_3 ($\lambda = 0.87$ Å) and D_2+NH_3 ($\lambda = 0.65$ Å). Explanation of the curves is given in fig. 8. The corresponding curves for H_2+NH_3 at $\lambda = 1.56$ Å are indistinguishable from those at $\lambda = 0.87$ Å, within plotting accuracy.

DISCUSSION

Ford and Wheeler [11] have shown by semi-classical techniques and for a central-field potential having an overall shape analogous to that of an LJ (12, 6) potential that when the deflection function has a relative extremum, interference between the attractive and repulsive branches leads to rapid oscillations superimposed on the broader supranumerary rainbow undulations. In the past, oscillations of the sort reported here have been described qualitatively as resulting from such an interference effect. This description is incorrect for our systems because in the quantum limit, where the de Broglie wavelength becomes comparable to the potential range, the Ford and Wheeler analysis is inapplicable. The breakdown of the semi-classical description is seen in at least two ways. First, we have observed strong undulations at angles considerably larger than the rainbow angle, whereas the semi-classical description predicts that oscillations die out rapidly on the dark side of the rainbow. For example, the LJ (12, 6) fit for the H_2+O_2 system predicts a classical rainbow at 15° in the CM, whereas we see strong oscillations out to 25°. Indeed, the absence of rainbows both in theory and experiment for these systems shows that the semi-classical approach cannot be used here. Second, accurate quantum mechanical theoretical calculations predict oscillations with a spacing given by eqn (1) for purely repulsive potentials with monotonic deflection functions.[18] The Ford and Wheeler analysis, however, reduces to the classical result whenever the deflection function is single-branched, and no undulations are possible. The oscillations in our systems are more accurately described as a diffraction effect produced at the steep repulsive wall of the potential.[19] The presence of an attractive well intensifies the diffraction oscillations and can increase their frequency since in this case the appropriate range parameter to use in eqn (1) is r_m rather than σ. However, since in most cases the van der Waals minimum occurs at a distance r_m only slightly larger than the zero of the potential, the frequency of the undulations is only slightly affected by the presence of the well.

The intermolecular potentials of the systems we have studied are anisotropic;

consequently, the interpretation of our data is more complicated than for atom–atom scattering. One approximate way of coping with this difficulty is to separate the potential into a spherical and an anisotropic part. We then assume that the effect of the latter is unimportant due to a combination of rotational averaging and the likelihood that the decrease of the magnitude of this anisotropy with the intermolecular distance, r, is more rapid than that of the spherically symmetric part, making it already sufficiently small for the distance range sampled by the present experiments. A partial wave expansion can then be used to determine the isotropic part of the potential, as was done in the previous section. Such an analysis, however, is not necessarily correct since the anisotropy may dampen or " quench " the oscillations and possibly shift their locations. Rothe and Helbing [20] and Kramer and LeBreton [21] report quenching of the glory undulations in the total scattering cross section of alkali atoms by various large asymmetric molecules. On the other hand, Aquilante *et al.*[12] find no evidence for quenching in the glory scattering of D_2 by N_2 and several hydrocarbons. Also, Butz *et al.*[11] were able to fit the glory undulations in the total cross sections of He, HD and D_2 scattered by CH_4, N_2, O_2, NO and CO using a spherical Lennard-Jones (12, 6) potential. Only the CO_2 glories appeared slightly dampened, as compared with their theoretical calculations. Turning to the rainbow maximum, Anlauf *et al.*[22] found that for $Ar+N_2$ it was weaker than expected from a Lennard-Jones (n, 6) potential (with best fit obtained for $n = 20$), and attribute this difference to quenching. Similarly, Cavallini *et al.*[23] compared the rainbow of $Ar+N_2$ with that of Ar+Ar and attributed the dampening of its intensity and the shift of its position to higher angles to anisotropy effects. Tully and Lee,[24] after studying the same $Ar+N_2$ system, assume that the shift in the rainbow position to larger angles is negligible, but that the quenching is not, and get a slightly deeper well than Anlauf *et al.* Stolte [25] measured the total cross section of Ar+NO with the rotational quantum numbers of NO selected to be $J = M_J = \frac{3}{2}$ and $J = M_J = \frac{5}{2}$, and found that the anisotropic contribution to the total cross section is less than 1 %. Farrar and Lee [26] have seen rapid quantum oscillations in the differential elastic scattering cross section for the $p\text{-}H_2+p\text{-}H_2$ system, and were able to interpret their data using a central-field assumption. We now consider the theoretical calculations on anisotropy effects on differential elastic cross sections done so far.

Cross [27] found in an approximate semi-classical calculation, using a potential with an isotropic part similar to that of K+Kr that anisotropy can significantly quench glory, rainbow and " rapid " oscillations. However, Cross' theory, which is based on the Ford and Wheeler treatment of interference between different branches of the deflection function, is inapplicable to our systems where the undulations are produced to a large extent by diffraction at the steep repulsive wall of the potential. Furthermore, he assumes that the dependence of the isotropic and anisotropic parts of the potential is identical, an assumption subject to question. Finally, the systems treated in the present paper are more highly quantum than that considered by Cross, and the anisotropic effects are expected to be quantitatively different. Wagner and McKoy,[28] in an exact solution of the Schrödinger equation for the scattering of $Ar+H_2$, found no significant quenching or shifting of the rapid quantum undulations. However, their results provide only a lower estimate on these effects since H_2 is more isotropic than other diatomic molecules, and rotational transitions, which play an important role in quenching, are less likely for low energy collisions with H_2.

The range of intermolecular distances sampled in the present experiments, estimated by a semi-classical analysis as described in the previous section, and depicted in fig. 8 to 10 inclusive, includes part of the repulsive wall and the minimum in the attractive well. We conclude from the present experiments that in this range, and

for the hydrogen or deuterium systems considered, effects of anisotropy on the differential cross sections are negligible (within experimental error). This conclusion is based on the following observations. First, the potentials obtained were independent of their assumed mathematical form. Indeed, comparison of the results for the three-parameter LJ (n, 6) potential and the four-parameter MSV potential, as given in fig. 8 to 10 inclusive, shows that they are nearly equal, even though their mathematical form in the r-range sampled by the experiments is substantially different. Second, a variety of different secondary scattering partners were studied. We did not find a correlation between the amplitudes of the observed oscillations and the symmetry of the secondary molecule, as would have been expected for significant anisotropy effects. Third, both H_2 and D_2 were scattered by the same secondary molecule. If quenching and angular shifting of the undulations by the anisotropy in the potential were significant, they would be expected to be sensitive to the relative momentum, or wavelength, of the colliding molecules. The fitted potential parameters obtained using the central-field assumption for the two isotopes at the same relative collision energy should as a result be different but, as pointed out at the end of the previous section, these potentials are the same to within the experimental errors. Fourth, the potentials for H_2+SF_6 and H_2+NH_3 were determined at two different relative energies (see tables 1 and 2). The fitted parameters are in excellent agreement with each other, a necessary condition for validity of the central-field assumption. Finally, the p-H_2+SF_6 experiments yielded results identical to the n-H_2+SF_6 scattering at the same relative energy, to within experimental error, thus indicating the insensitivity of the measurements to the distribution of H_2 initial rotational states. In summary,

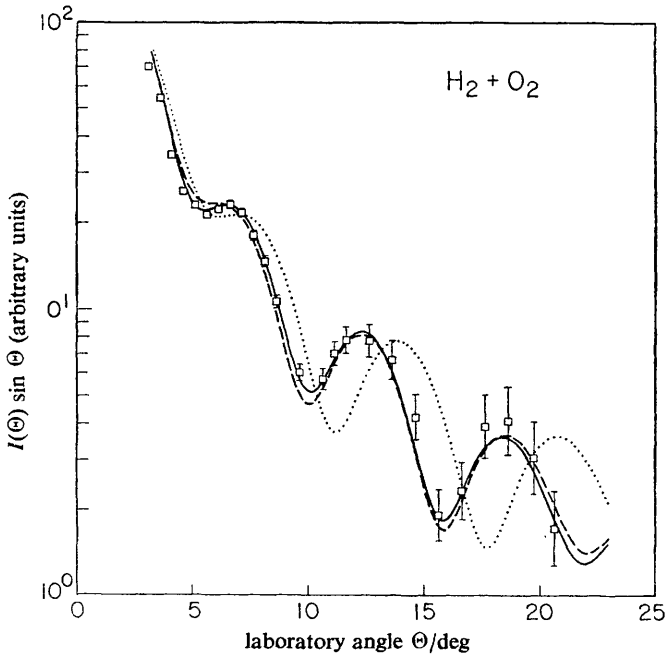

FIG. 11.—Comparison of the differential elastic scattering predicted by total cross section measurements with the experimental H_2+O_2 data from fig. 3. The solid curve represents the LJ (12, 6) fit given in table 1. The dotted curve was determined using the LJ (12, 6) ε and σ parameters of Butz *et al.*[11] given in table 3, while the dashed curve was fitted to the data using the $\varepsilon\sigma$ product determined by Butz *et al.*

we have found it possible in every case to describe the measured differential elastic scattering cross sections using a spherically symmetric potential which is independent of the de Broglie wavelength λ of the experiment.

Both the position and the amplitude of the rapid oscillations, as well as the overall shape of the cross section are accurately fitted by such spherical potentials; no effects of anisotropy are observed.

Butz *et al.*[11] have fitted a LJ (12, 6) potential to their total cross section measurements of D_2+O_2, D_2+CO and D_2+CH_4. The total cross section results yield the product $\varepsilon\sigma$, but do not give reliable estimates for the individual parameters. Aquilante *et al.*'s results [12] for D_2+CH_4 agree with those of Butz *et al.* To compare the latter's results with our own, we have used their $\varepsilon\sigma$ product values and determined the individual parameters by the Newton's method described in the previous section.

TABLE 3.—COMPARISON WITH LJ (12, 6) PARAMETERS OBTAINED FROM TOTAL CROSS SECTION MEASUREMENTS

system	σ/Å	ε/meV	ref.
H_2+O_2	3.38±0.03	7.7±0.9	this work
	2.99	6.3	ref. (11)
	3.37±0.05	5.6±1.2	(a)
H_2+CO	3.5±0.1	6.9±1.5	this work
	3.11	5.7	ref. (11)
	3.41±0.4	5.2±1.5	(a)
H_2+CH_4	3.7±0.2	9.9±1.4	this work
	2.95	7.4	ref. (11)
	3.52±0.3	6.2±2.0	(a)
	3.6	6.0	ref. (12)
	3.53±0.3	6.2±2.0	(a)

(a) These values were obtained by holding the product $\varepsilon\sigma$ constant, while allowing σ to vary to give a best fit to the experimental data.

Based on our previous conclusions that the H_2 and D_2 isotopes yield the same scattering potentials, these calculations were done for the H_2+O_2, H_2+CO and H_2+CH_4 systems in which the quantum undulations are more pronounced. The results of these restricted fits are given in table 3, together with the unrestricted ones, as well as those obtained by Butz *et al.*, from their total cross sections. The corresponding differential cross sections are shown in fig. 11 for H_2+O_2. In addition, our LJ (12, 6) best fit cross section is reproduced for comparison. It is clear that neither the total cross section data, nor the best fit obtained using the constrained product of $\varepsilon\sigma$ give as good an agreement as the unconstrained LJ (12, 6) fit. While this is true for all of the systems compared, it should be noted that the results obtained from the constrained fit are in much better agreement with the differential cross section data than are the predictions from the separate parameters obtained from the total cross sections. This emphasizes the value of total cross section measurements in determining $\varepsilon\sigma$ product values, while giving less reliable estimates of the separate parameters. In contrast, differential cross section measurements of the type reported here yield a more accurate description of the intermolecular potential, indicating among other things deviations from the LJ (12, 6) expression, as shown from the $H_2(D_2)+O_2$ system in fig. 3.

In concluding, it should be remarked that the lack of anisotropy effects for the $H_2(D_2)$-containing systems described in the present paper, are probably due at least in part to the fact that this molecule is nearly spherical. In addition, rotational excita-

tion processes probably result from small orbital angular momenta and manifest themselves at large scattering angles, in a manner determined mainly by the intermolecular potential at distances shorter than those sampled in the present experiments. One should be extremely cautious in attempting to extend these conclusions to other systems.

[1] See for example, J. Amdur and J. B. Jordan, *Adv. Chem. Phys.*, X (Interscience, New York, 1966), pp. 29-74 and references cited therein.
[2] A. J. H. Boerboom, H. Van Dop and J. Los, *Physica*, 1970, **46**, 458.
[3] Yw. N. Belayev, N. V. Kamyshon, V. B. Leonas and A. V. Smeryagin, *Entropie*, 1969, **30**, 173.
[4] The same is true for differential cross sections. See, for example, William H. Miller, *J. Chem. Phys.*, 1969, **51**, 3631.
[5] U. Buck and H. Pauly, *J. Chem. Phys.*, 1971, **54**, 1929.
[6] Daniel H. Winicur, A. L. Morsund, W. R. Devereaux, L. R. Martin and Aron Kuppermann, *J. Chem. Phys.*, 1970, **52**, 3299.
[7] M. Cavallini, L. Meneghetti, G. Scoles, and M. Yealland, *Phys. Rev. Letters*, 1970, **24**, 1469.
[8] D. Auerbach, C. Detz, K. Reed and L. Wharton, *Abstracts from VII ICPEAC* (North-Holland, Amsterdam, 1971), pp. 541-542.
[9] J. M. Farrar and Y. T. Lee, *J. Chem. Phys.*, 1972, **56**, 5801, and earlier papers cited therein.
[10] See, for example, Richard B. Bernstein, *Adv. Chem. Phys.*, X (Interscience, New York, 1966), p. 100, eqn (VI.6), with $L_a \sim L_0 \sim (\mu v b/\hbar)$.
[11] H. P. Butz, R. Feltgen, H. Pauly and H. V. Vehmeyer, *Z. Phys.*, 1971, **247**, 70.
[12] V. Aquilante, G. Liuti, F. Vecchio-Cattivi and G. G. Volpi, *Mol. Phys.*, 1971, **21**, 1149.
[13] Extranuclear Laboratories, Inc., Pittsburgh, Pennsylvania.
[14] W. Paul and H. Steinwedel, *Z. Naturforsch.*, 1953, **8a**, 448.
[15] P. E. Siska, J. M. Parson, T. P. Schafer and Y. T. Lee, *J. Chem. Phys.*, 1971, **55**, 5762.
[16] D. W. Marquardt, *J. Soc. Ind. Appl. Math.*, 1963, **11**, 431.
[17] Kenneth W. Ford and John A. Wheeler, *Ann. Phys.*, 1959, **7**, 259.
[18] John Adams, *Ph.D. Thesis* (University of Arkansas, 1969).
[19] Robert J. Gordon and Martin Griss, to be published.
[20] Erhard W. Rothe and Reinhard K. B. Helbing, *J. Chem. Phys.*, 1970, **53**, 2501.
[21] H. L. Kramer and P. R. LeBreton, *J. Chem. Phys.*, 1967, **47**, 3367.
[22] K. G. Anlauf, R. Bickes Jr., and R. B. Bernstein, *J. Chem. Phys.*, 1971, **54**, 3647.
[23] M. Cavallini, M. G. Dondi, G. Scoles and U. Valbusa, *Chem. Phys. Letters*, 1971, **10**, 22.
[24] F. P. Tully and Y. T. Lee, *J. Chem. Phys.*, 1972, **57**, 866.
[25] Steven Stolte, *Ph.D. Thesis* (Catholic University of Nijmegen, 1972).
[26] J. M. Farrar and Y. T. Lee, *J. Chem. Phys.*, 1972, **57**, 5492.
[27] R. J. Cross, *J. Chem. Phys.*, 1970, **52**, 5703.
[28] A. F. Wagner and V. McKoy, *J. Chem. Phys.*, 1973, **58**.